Heterogeneous Catalysis

Deutsche Ausgabe: DOI: 10.1002/ange.201412052
Internationale Ausgabe: DOI: 10.1002/anie.201412052

Probing the Coordinative Unsaturation and Local Environment of Ti^{3+} Sites in an Activated High-Yield Ziegler–Natta Catalyst**

*Elena Morra, Elio Giamello, Sabine Van Doorslaer, Giuseppe Antinucci, Maddalena D'Amore, Vincenzo Busico, and Mario Chiesa**

Abstract: *The typical activation of a fourth generation Ziegler–Natta catalyst $TiCl_4/MgCl_2$/phthalate with triethyl aluminum generates Ti^{3+} centers that are investigated by multi-frequency continuous wave and pulse EPR methods. Two families of isolated, molecule-like Ti^{3+} species have been identified. A comparison of the experimentally derived g tensors and $^{35,37}Cl$ hyperfine and nuclear-quadrupole tensors with DFT-computed values suggests that the dominant EPR-active Ti^{3+} species is located on $MgCl_2$(110) surfaces (or equivalent $MgCl_2$ terminations with tetra-coordinated Mg). O_2 reactivity tests show that a fraction of these Ti sites is chemically accessible, an important result in view of the search for the true catalyst active site in olefin polymerization.*

Despite major research efforts, $MgCl_2$-supported Ziegler–Natta (ZN) catalyst systems for the industrial production of isotactic polypropylene[1] remain elusive. Efforts have been made to characterize model systems[2,3] but no direct insight into the complex, polycrystalline working catalysts at the molecular level has been obtained to date. Progress has been made in the elucidation of the $MgCl_2$ surface structure and stability[4] and periodic DFT studies have suggested that $MgCl_2$(110) terminations are the only surfaces where $TiCl_4$ (the most common precursor of the active species) can lead to moderately stable adsorbates.[5] The influence of certain Lewis bases and at a later stage the AlR_3 cocatalyst[1] on the system is still largely unestablished and seminal experimental[3,6–9] and theoretical[5,10–14] investigations have failed to account for all known facts. Activation is usually performed by reacting the precatalyst with aluminum alkyl compounds (typically triethyl aluminum, TEA). In this process tetravalent Ti^{4+} ions assume a lower oxidation state[15] and both Ti^{3+} and Ti^{2+} ions have been proposed. Ti^{3+} centers are believed to play an important role in ZN catalysis, however their exact role and nature is still uncertain.

As a result of the paramagnetic nature of the Ti^{3+} center ($3d^1$, $S = 1/2$), electron paramagnetic resonance (EPR) is the ideal technique to unravel the nature and local coordinative environment of these sites. Conventional X-band continuous-wave (CW) EPR techniques have been used primarily to monitor the amount of reduced Ti species.[16–21] However, modern EPR techniques offer a whole arsenal of specific experiments capable of investigating the local environment of paramagnetic species. Herein, we employ a combination of multi-frequency CW and pulse EPR experiments, complemented with DFT calculations, to elucidate the nature and reactivity of Ti^{3+} centers generated by reacting a fourth generation $MgCl_2/TiCl_4$/dibutylphthalate precatalyst (Ti 2.0% by weight and dibutylphthalate 8.9% by weight) with TEA vapors.[1]

The catalyst activation was performed in situ by exposing a weighted amount of precatalyst (typically 0.06 g) to TEA vapors in a specially designed cell (described elsewhere).[22]

Upon reaction with TEA vapors the sample underwent a slight color change from dark yellow to pale brown and an intense EPR signal appeared. The X- and W-band CW EPR spectra are reported in Figure 1a and 1b respectively. The spectra show the typical g values (Table 1) expected for a system with a singly occupied molecular orbital (SOMO) which is composed predominantly of a 3d orbital of Ti. Quantification of the EPR signal in Figure 1 indicates that the amount of EPR-active Ti^{3+} species is of the order of 15 ± 5% of the total Ti content. The g tensor elements were determined by computer simulation of the spectra at the two frequencies (Figure 1), indicating the presence of three species (Table 1). Two of them (S1 and S2), with different relative contributions, account for the majority of the spectral intensity. The relative abundance of the three species was found to vary slightly from experiment to experiment. Both set of g values for the principal species (S1 and S2) are in line with reported values for Ti^{3+} species observed in ZN catalysts.[23]

To probe the local environment of the Ti^{3+} species, hyperfine sublevel correlation spectroscopy (HYSCORE) experiments at the Q-band frequency were performed (no electron spin echo was detected at the X-band frequency).

The Q-band HYSCORE spectrum (Figure 1c) is dominated by correlation peaks at (6, 2.8) and (2.8, 6) MHz arising

[*] E. Morra, Prof. E. Giamello, Prof. M. Chiesa
Dipartimento di Chimica and NIS, Università degli Studi di Torino
Via Giuria 7, 10125 Torino (Italy)
E-mail: mario.chiesa@unito.it
E. Morra
Dutch Polymer Institute(DPI)
P.O. Box 902, 5600 AX Eindhoven (The Netherlands)
E. Morra, Prof. S. Van Doorslaer
Department of Physics, University of Antwerp
Universiteitsplein 1, B-2610 Antwerp-Wilrijk (Belgium)
G. Antinucci, Dr. M. D'Amore, Prof. V. Busico
Dipartimento di Scienze Chimiche
Università degli Studi di Napoli Federico II
Via Cintia 21, 80126 Napoli (Italy)

[**] This work is part of the research program of the Dutch Polymer Institute (DPI), project number 754. We acknowledge Dr. Sara Maurelli for recording some of the HYSCORE spectra. We are grateful to SABIC for donating the precatalyst.

Supporting information for this article is available on the WWW under http://dx.doi.org/10.1002/anie.201412052.

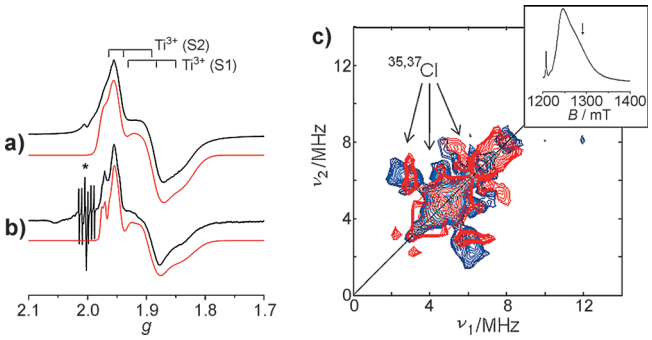

Figure 1. a) Experimental (black) and simulated (red) X-band CW EPR spectra of the activated catalyst. b) W-band CW EPR spectra of the same sample. Spectra were recorded at $T = 77$ K. The asterisk indicates a Mn^{2+} impurity. c) Q-band experimental (blue) and simulated (red) HYSCORE spectra measured at the position indicated in the inset ($B_0 = 1290.0$ mT), showing ^{35}Cl and ^{37}Cl signals. The spectral deconvolution of (a) and (b), the HYSCORE spectrum recorded at the maximum echo intensity, and the complete experimental details are reported in the Supporting Information.

from the hyperfine interaction with ^{35}Cl and ^{37}Cl nuclei. Given the superposition of the spectral features of S1 and S2, the HYSCORE spectra reflect hyperfine and nuclear quadrupole interactions associated with both Ti^{3+} species.

For the simulation of the HYSCORE spectrum, spin Hamiltonian parameters, recently obtained for $TiCl_3$ molecular complexes,[24] and the results of DFT computations (see below) were used as starting values. An example of a reasonable simulation is shown in Figure 1 c (see also the Supporting Information). The main feature of the experimental spectra could be reproduced by considering a Cl hyperfine-interaction tensor characterized by a fairly large dipolar component and relatively small Fermi contact contributions and nuclear-quadrupole-interaction values (e^2qQ/h) in the range 6–12 MHz. These values are in line with experimental and computed values for molecular complexes in which Cl is directly coordinated to a Ti^{3+} center.[24] The same spin Hamiltonian parameters have been used to fit W-band ELDOR-detected NMR spectra, which are reported in the Supporting Information (ELDOR = electron double resonance).

To interpret the spectroscopic data in terms of microscopic models, DFT calculations have been carried out (details in Supporting Information). Two models representative of Ti^{3+} on the (110) and (104) $MgCl_2$ surfaces have been considered (Figure 2 a and b, respectively). The DFT-computed spin Hamiltonian parameters are reported in Table 2. The hyperfine-interaction tensors show a large dipolar character with consistent departure from axial symmetry in line with a large spin density in the Cl p orbitals.

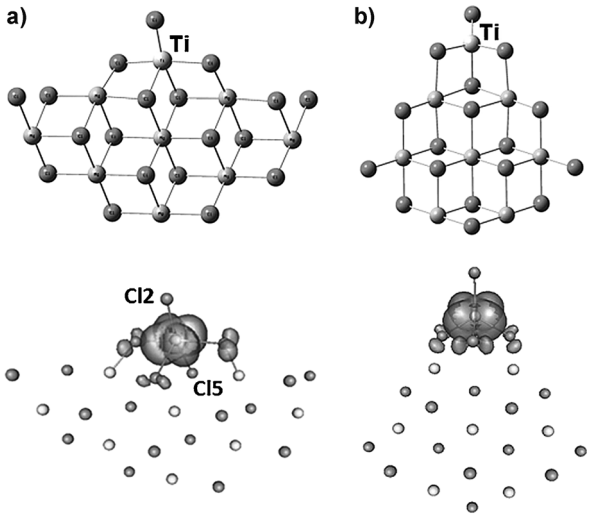

Figure 2. DFT model structures and corresponding spin density plots of $TiCl_3$ localized at a) $MgCl_2$(110) surfaces and b) $MgCl_2$(104) surfaces. Spin densities are displayed for an isosurface value of 0.002.

Overall the computed hyperfine and nuclear-quadrupole Cl tensors are compatible with the experimental HYSCORE spectrum and concur with the results obtained on $TiCl_3$ molecular complexes.[24] The computed g tensors for the two models are consistent with the single electron occupying a d_{xy} or $d_{x^2-y^2}$ orbital (Figure 2). Distinctly different g tensor elements are computed for the two models, with the case of the tetra-coordinated Ti^{3+} located at the $MgCl_2$(110) surface (Figure 2 a) being in better agreement with the experimental values relative to the most abundant Ti^{3+} species (S1).

The experiments illustrated in Figure 1 thus show that the reaction of the precatalyst with TEA yielded isolated molecule-like Ti^{3+} species with directly bound Cl ions. The

Table 1: Spin Hamiltonian parameters extracted from computer simulation of the experimental spectra reported in Figures 1 and 3.[a]

		g_1	g_2	g_3	%ab		A_1	A_2	A_3	α,β,γ	e^2qQ/h	η	α',β',γ'
Ti^{3+}	S1	1.936 ± 0.01	1.888 ± 0.01	1.84 ± 0.01	76	^{35}Cl	−3.5 ± 1.5	−0.5 ± 2.5	7.0 ± 3.5	90,46,50 ± 20	−9 ± 3	0.3 ± 0.2	10,55,0 ± 20
	S2	1.960 ± 0.01	1.945 ± 0.01	1.89 ± 0.01	23								
	S3	1.976 ± 0.005	1.968 ± 0.005	1.96 ± 0.01	1								
						^{1}H	0.5 ± 0.3	0.5 ± 0.3	8.5 ± 0.5	0,90,0 ± 5			
O_2^-		2.0035 ± 0.0002	2.0106 ± 0.0002	2.0209 ± 0.0002	100	^{27}Al	8 ± 1	8 ± 1	11 ± 1	—			

[a] The g-matrix principal values were determined from the simultaneous simulation of the X- and W-band CW EPR spectra, while the hyperfine parameters were determined from simulations of HYSCORE data (Figure 1 and Figure 3, as well as the Supporting Information). The Euler angles α, β, γ (°) define the passive rotation of the hyperfine and quadrupole principal axes system into the g-matrix principal axes system, $A = R(\alpha,\beta,\gamma)\, A_{diagonal} R^{+}(\alpha,\beta,\gamma)$. Signs of the proton hyperfine elements are based on the point-dipole model. All hyperfine-interaction and nuclear-quadrupole-interaction values are given in MHz.

Table 2: Computed DFT spin Hamiltonian parameters for the models reported in Figure 2.[a]

	g_x	g_y	g_z	^{35}Cl	A_x	A_y	A_z	e^2qQ/h	η
$TiCl_3/MgCl_2(110)$	1.888	1.788	1.939	Cl1	−3.6	−2.8	−1.9	−8.4	0.83
				Cl2	−2.7	0.07	10.6	−14.1	0.56
				Cl3	−5.2	−1.9	10.1	−12.4	0.87
				Cl4	−3.6	−0.6	5.6	−9.8	0.57
				Cl5	−1.0	0.5	0.8	−9.6	0.2
$TiCl_3/MgCl_2(104)$	1.850	1.968	1.909	Cl1	−3.7	−1.6	8.9	−10.4	0.34
				Cl2	−6.1	−3.0	5.1	−8.6	0.13
				Cl3	−3.8	−1.7	9.6	−10.4	0.41
				Cl4	−3.9	−3.7	1.1	5.7	0.77

[a] All hyperfine-interaction and nuclear-quadrupole-interaction values are given in MHz.

observation of well-defined molecule-like sites in an industrial heterogeneous catalyst is in itself remarkable, considering the complexity of the system. A comparison between experimental and DFT-computed EPR parameters suggests that the dominant EPR-active Ti^{3+} species is characterized by a well-defined and homogeneous environment, compatible with $MgCl_2(110)$ or equivalent surfaces.

The important question arises as to whether the isolated Ti^{3+} centers detected by EPR are chemically accessible or not. To answer this question the sample was reacted with molecular oxygen (50 mbar at room temperature). Oxygen is a well-known electron scavenger and readily reacts with a Ti^{3+} center according to Equation (1):

$$Ti^{3+} + O_{2(gas)} \rightarrow O_2^{-}{}_{(ads)} + Ti^{4+} \quad (1)$$

Upon reaction with O_2 (Figure 3a), we observe a consistent decrease of the Ti^{3+} signal (down to ≈60% of the initial intensity) and the appearance of the spectrum of surface-adsorbed O_2^- species. The *g* matrix (Table 1) is typical for an ionic superoxide species stabilized at a Ti^{4+} site.[25–29] Remarkably, the Q-band EPR spectrum (Figure 3b) indicates that one single O_2^- species was formed, implying a single stabilizing Ti^{4+} surface site. The presence of residual Ti^{3+} sites (≈40% of the EPR-active Ti^{3+} species) in turn indicates that the activation process also gave rise to Ti^{3+} species which are chemically inactive under the mild experimental conditions, because of coordinative saturation and/or because they are buried underneath the catalyst surface.

The O_2^- ions can also be exploited as paramagnetic probes to further monitor the local environment of the adsorption site. In particular X- and Q-band HYSCORE spectra (Figure 3c,d) allowed us to resolve hyperfine-interaction coupling constants with nearby ^{1}H, ^{27}Al, and ^{35,37}Cl nuclei.

A ^{1}H X-band HYSCORE spectrum of the formed O_2^- radicals is shown in Figure 3c. Simulation of the spectra recorded at different magnetic-field settings (Supporting Information) provided the full hyperfine matrix (Table 1), from which a O_2^-–H distance of 0.33 nm can be estimated using the point dipole approximation. This proton may have different sources and we cannot make a definitive assignment at this stage.

The Q-band HYSCORE spectrum (Figure 3d) shows the presence of signals attributable to ^{35}Cl, ^{37}Cl, and ^{27}Al nuclei. The most interesting features are the ^{27}Al cross peaks, separated by approximately 10 MHz, indicating a large isotropic (Fermi contact) contribution and direct interaction of the radical with a nearby Al ion (see the Supporting Information for a detailed analysis). A similar case was found for O_2^- radicals generated at the surface of MgO doped with Na atoms.[30] Figure 4 presents a proposed O_2^- radical coordination at the adsorption site and interaction with a nearby Al ion which may explain the experimental results obtained herein.

In summary, monomeric and well-defined EPR-active Ti^{3+} species are formed by activating an industrial $MgCl_2$-supported ZN precatalyst with TEA. These species account for approximately 15% of the total Ti content and are

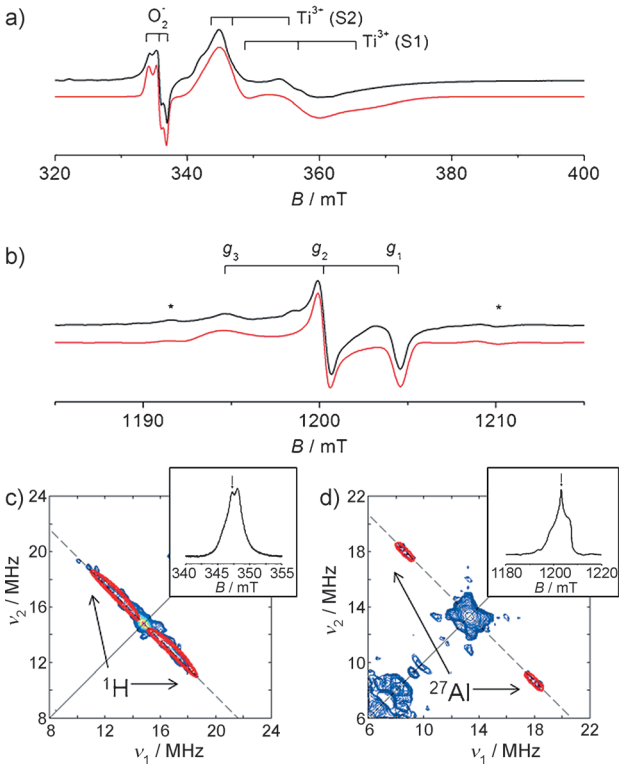

Figure 3. Experimental (black/blue) and simulated (red) spectra recorded upon reaction at room temperature of the activated catalyst with molecular O_2. a) X-band CW EPR spectrum recorded at 77 K. b) Q-band FID-integral-detected EPR spectrum of the superoxide radical anion recorded at 40 K. To facilitate the comparison with the CW X-band spectrum the first derivative of the absorption is presented. The asterisks indicate a Mn^{2+} impurity. c) ^{1}H X-band HYSCORE spectrum of the surface O_2^-, recorded at the position indicated in the inset (B_0 = 347.3 mT). d) ^{27}Al Q-band HYSCORE spectrum recorded at the position indicated in the inset (B_0 = 1200.5 mT). All HYSCORE spectra were recorded at 40 K. The spin Hamiltonian parameters used in the simulations are listed in Table 1. The full set of spectra is shown in the Supporting Information.

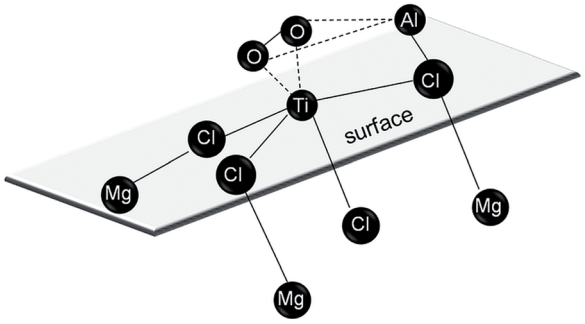

Figure 4. The proposed O_2^- radical coordination and interactions at the adsorption site. The proton is omitted for clarity.

characterized by a well-defined environment compatible with $MgCl_2(110)$ or equivalent surfaces exposing tetra-coordinated Mg ions. Only a fraction ($\approx 60\,\%$) of these Ti^{3+} species is chemically accessible and reacts via an electron-transfer mechanism with O_2. A fraction of the reacted oxygen is stabilized on Ti^{4+} sites in the form of surface O_2^- radical ions in proximity to Al^{3+} ions.

In conclusion, we demonstrated the presence of a non-negligible amount of Ti^{3+} species in the form of monomeric isolated and chemically accessible centers. Even though we have, at present, no evidence that these are the actual catalytic sites operating in heterogeneous ZN catalysts, this is the first time that Ti^{3+} centers formed upon activation of a heterogeneous industrial ZN catalyst are characterized at a molecular level. This accomplishment is a crucial step towards the identification of potential active sites in heterogeneous ZN catalysts and the resolution of one of the most exciting open problems of modern catalysis.

Keywords: EPR spectroscopy · heterogeneous catalysis · polymerization · titanium · Ziegler–Natta catalysts

How to cite: *Angew. Chem. Int. Ed.* **2015**, *54*, 4857–4860
Angew. Chem. **2015**, *127*, 4939–4942

[1] E. Albizzati, U. Giannini, G. Collina, L. Noristi, L. Resconi in *Polypropylene Handbook: Catalysts and Polymerizations* (Ed.: E. P. Moore, Jr.), Hanser-Gardner Publications, Cincinnati, **1996**, Chapter. 2.
[2] T. Risse, J. Schmidt, H. Hamann, H. J. Freund, *Angew. Chem. Int. Ed.* **2002**, *41*, 1517–1520; *Angew. Chem.* **2002**, *114*, 1587–1591.
[3] a) E. Magni, G. A. Somorjai, *J. Phys. Chem.* **1996**, *100*, 14786–14793; b) E. Magni, G. A. Somorjai, *Catal. Lett.* **1995**, *35*, 205–214; c) S. H. Kim, G. A. Somorjai, *Surf. Interface Anal.* **2001**, *31*, 701–710.
[4] V. Busico, M. Causà, R. Cipullo, R. Credendino, F. Cutillo, N. Friederichs, R. Lamanna, A. Segre, V. Van Axel Castelli, *J. Phys. Chem. C* **2008**, *112*, 1081–1089.
[5] M. Seth, P. M. Margl, T. Ziegler, *Macromolecules* **2002**, *35*, 7815–7829.
[6] P. Corradini, V. Barone, R. Fusco, G. Guerra, *Gazz. Chim. Ital.* **1983**, *113*, 601–607.
[7] H. Mori, M. Sawada, T. Higuchi, K. Hasebe, N. Otsuka, M. Terano, *Macromol. Rapid Commun.* **1999**, *20*, 245–250.
[8] L. Brambilla, G. Zerbi, F. Piemontesi, S. Nascetti, G. Morini, *J. Mol. Catal. A* **2007**, *263*, 103–111.
[9] T. Taniike, S. Takahashi, T. Wada, K. Tonosaki, S. Dwivedi, M. Terano, *Macromol. Symp.* **2012**, *313*, 1–7.
[10] M. Boero, M. Parrinello, H. Weiss, S. Huffer, *J. Phys. Chem. A* **2001**, *105*, 5096–5105.
[11] D. V. Stukalov, I. L. Zilberberg, V. A. Zakharov, *Macromolecules* **2009**, *42*, 8165–8171.
[12] T. Taniike, M. Terano, *Macromol. Rapid Commun.* **2008**, *29*, 1472–1476.
[13] N. Bahri-Laleh, A. Correa, S. Mehdipour-Ataei, H. Arabi, M. N. Haghighi, G. Zohuri, L. Cavallo, *Macromolecules* **2011**, *44*, 778–783.
[14] M. D'Amore, R. Credendino, P. H. M. Budzelaar, M. Causà, V. Busico, *J. Catal.* **2012**, *286*, 103–110.
[15] C. Beermann, H. Bestian, *Angew. Chem.* **1959**, *71*, 618–623.
[16] P. Brant, A. N. Speca, *Macromolecules* **1987**, *20*, 2740–2744.
[17] J. C. W. Chien, J. C. Wu, C. I. Kuo, *J. Polym. Sci. Part A* **1982**, *20*, 2019–2032.
[18] P. Šindelář, D. Matula, J. Holeček, *J. Polym. Sci. Part A* **1996**, *34*, 2163–2171.
[19] V. A. Poluboyarov, V. F. Anufrienko, V. A. Zakharov, S. A. Sergeev, S. I. Makhtarulin, G. D. Bukatov, *React. Kinet. Catal. Lett.* **1984**, *26*, 347–351.
[20] A. A. Tregubov, V. A. Zakharov, T. B. Mikenas, *J. Polym. Sci. Part A* **2009**, *47*, 6362–6372.
[21] E. I. Koshevoy, T. B. Mikenas, V. A. Zakharov, A. M. Volodin, R. M. Kenzhin, *Catal. Commun.* **2014**, *48*, 38–40.
[22] E. Morra, E. Giamello, M. Chiesa, *Chem. Eur. J.* **2014**, *20*, 7381–7388.
[23] J. C. W. Chien, Y. Hu, *J. Polym. Sci. Part A* **1989**, *27*, 897–913.
[24] S. Maurelli, E. Morra, S. Van Doorslaer, V. Busico, M. Chiesa, *Phys. Chem. Chem. Phys.* **2014**, *16*, 19625–19633.
[25] A. M. Prakash, V. Kurshev, L. Kevan, *J. Phys. Chem. B* **1997**, *101*, 9794–9799.
[26] K. L. Antcliff, D. M. Murphy, E. Griffiths, E. Giamello, *Phys. Chem. Chem. Phys.* **2003**, *5*, 4306–4316.
[27] Z. Sojka, *Catal. Rev. Sci. Eng.* **1995**, *37*, 461–512.
[28] M. Che, A. J. Tench, *Adv. Catal.* **1983**, *32*, 1–148.
[29] F. Geobaldo, S. Bordiga, A. Zecchina, E. Giamello, G. Leofanti, G. Petrini, *Catal. Lett.* **1992**, *16*, 109–115.
[30] F. Napoli, M. Chiesa, E. Giamello, G. Preda, C. Di Valentin, G. Pacchioni, *Chem. Eur. J.* **2010**, *16*, 6776–6785.

Received: December 16, 2014
Revised: January 30, 2015
Published online: February 23, 2015